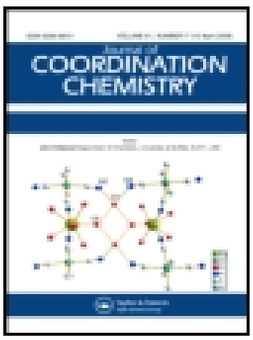

Journal of Coordination Chemistry

ISSN: 0095-8972 (Print) 1029-0389 (Online) Journal homepage: http://www.tandfonline.com/loi/gcoo20

Silver(I) complex with 2-amino-4,4α-dihydro-4α,7-dimethyl-3H-phenoxazin-3-one (Phx-1) ligand: Crystal structure, vibrational spectra and biological studies

K. Helios, H. Maniak, M. Sowa, W. Zierkiewicz, M. Wąsińska-Kałwa, M. Giurg, P. Drożdżewski, A. Trusek-Hołownia, M. Malik & K. Krauze

To cite this article: K. Helios, H. Maniak, M. Sowa, W. Zierkiewicz, M. Wąsińska-Kałwa, M. Giurg, P. Drożdżewski, A. Trusek-Hołownia, M. Malik & K. Krauze (2017): Silver(I) complex with 2-amino-4,4α-dihydro-4α,7-dimethyl-3H-phenoxazin-3-one (Phx-1) ligand: Crystal structure, vibrational spectra and biological studies, Journal of Coordination Chemistry, DOI: 10.1080/00958972.2017.1384822

To link to this article: http://dx.doi.org/10.1080/00958972.2017.1384822

Accepted author version posted online: 26 Sep 2017.

Publisher: Taylor & Francis
Journal: *Journal of Coordination Chemistry*
DOI: http://doi.org/10.1080/00958972.2017.1384822

Silver(I) complex with 2-amino-4,4α-dihydro-4α,7-dimethyl-3*H*-phenoxazin-3-one (Phx-1) ligand: Crystal structure, vibrational spectra and biological studies

K. HELIOS, H. MANIAK, M. SOWA, W. ZIERKIEWICZ, M. WĄSIŃSKA-KAŁWA, M. GIURG, P. DROŻDŻEWSKI*, A. TRUSEK-HOŁOWNIA, M. MALIK and K. KRAUZE

Faculty of Chemistry, Wrocław University of Technology, Wybrzeże Wyspiańskiego 27, 50-370 Wrocław, Poland

The first metal complex of Phx-1 ligand, bis(2-amino-4,4α-dihydro-4α,7-dimethyl-3*H*-phenoxazin-3-one)nitratosilver(I), $[Ag(Phx\text{-}1)_2NO_3]$, has been obtained and investigated by single crystal X-ray diffraction and vibrational spectroscopy methods. The Ag^+ is bonded to heterocyclic nitrogen atoms of two organic ligands and one oxygen atom of a nitrate anion. The Phx-1 ligand coordination mode is supported by IR and Raman spectra, interpreted with the help of theoretical DFT studies. The antibacterial activity of the ligand and its Ag(I) complex as well as some reference compounds were screened against Gram-positive and Gram-negative bacteria, applying microdilution procedures. High sensitivity to the studied complex was found for *R. erythropolis* and *B. licheniformis* strains. Modified Phx-1 ligand preparation procedures are also presented.

Keywords: Phenoxazine-3-one derivative; Ag Complex; Crystal and molecular structure; Infrared and Raman spectra; Vibrational assignment; DFT

1. Introduction

Recently, the aminophenoxazin-3-ones have attracted growing attention in medicine. The simplest 2-aminophenoxazin-3-one (Questiomycin A, Phx-3) is a naturally occurring heterocycle and it is the key part of Actinomycin D (figure 1), the first antibiotic with anticancer properties [1]. Results obtained by Tomoda and coworkers [2] indicate that Phx-3 has the potential to

*Corresponding author. Email: piotr.drozdzewski@pwr.edu.pl

promote apoptosis of cancer cells, and may be applied to treat gastric and colon cancer, which are refractory to chemotherapy. The methyl derivative of Phx-3, 2-amino-4,4α-dihydro-4α,7-dimethyl-3*H*-phenoxazin-3-one (Phx-1), used here gives *in vitro* and *in vivo* antitumor effects against the human retinoblastoma cell line Y79 [3]. Phx-1 and Phx-3 exert anticancer activity against human pancreatic cancer cell lines, KLM-1 and MIA-PaCa-2 [4]. Other studies have shown that Phx-1, Phx-2 and Phx-3 may be useful as therapeutic agents against adult T-cell leukemia (ATL), a malignant tumor of human CD4+ T cells infected with a human retrovirus, T lymphotropic virus type-1 (HTLV-1) [5]. *In vivo* antiviral studies of activities against herpes viruses (HSV) intravaginally inoculated into mice have been made and show promising data that Phx-1, Phx-2 and Phx-3 are attractive candidates for agents to prevent replication of HSV and aggravation of lesions caused by these viruses [6]. Also, the antibacterial activity of Phx-1, Phx-2 and Phx-3 have been investigated. All presented derivatives show prominent antimicrobial activity against non-tuberculosis mycobacterial strains, *M. scrofulaceum*, *M. kansasii*, *M. marinum* and *M. intracellurale* [7].

In addition to the extensive studies of the biological activities of 2-aminophenoxazin-3-ones, the properties of well-dispersed PtRu and Pd nanoparticles on Phx-3 functionalized multi-walled carbon nanotubes (MWCNTs) have been reported and the results are very promising for portable applications in direct methanol fuel cells (DMFCs) field [8, 9]. Until now only one metal complex with Phx-3, ([Ag(Phx-3)NO_3]) and its enhanced (in comparison to free ligand) biological activity against *S. aureus* have been reported [10].

In this article we report the synthesis, crystal structure, Raman and IR spectra with band assignments made on the basis of theoretical calculations of the first metal complex with Phx-1, [Ag(Phx-1)$_2NO_3$]. Its biological activity has also been tested in order to validate the idea that binding the metal by some ligands may enhance their biological activity.

Prior to the complex preparation, the Phx-1 ligand was obtained via two modified click procedures using the corresponding 2-amino-5-methylphenol and hydrogen peroxide (H_2O_2) in the presence of ebselen or horseradish peroxidase (HRP).

2. Experimental

2.1. *Materials and methods*

All solvents were distilled before use. Commercially available reagents, 2-amino-5-

methylphenol, DMSO (Aldrich), $AgNO_3$ and aqueous hydrogen peroxide (H_2O_2) (Avantor Performance Materials Poland S.A.), and Horseradish Peroxidase catalyst (HRP) (Sigma), were used without purification. Water for enzymatic transformation was distilled twice.

Analytical TLC was performed on PET foils precoated with silica gel (Merck silica gel, 60 F254) and were made visual under UV light (λ_{max} = 254 nm). Melting points were determined on an Electrothermal IA 91100 digital melting point apparatus using the standard open capillary method.

2.2. *Syntheses*

2.2.1. Preparation of the Phx-1 ligand. An exhaustive literature survey showed that the preparation of Phx-1 required 2-amino-5-methylphenol [11, 12] and 2-nitro-5-methylphenol [13]. However, no multigram scale procedures were described to date. Prior to the complex preparation, the Phx-1 ligand was obtained in gram scale via two modified click procedures using the corresponding 2-amino-5-methylphenol and hydrogen peroxide (H_2O_2) in the presence of ebselen or horseradish peroxidase (HRP); see Supporting Information for details.

2.2.2. Preparation of the silver complex - bis(2-amino-4,4α-dihydro-4α,7-dimethyl-3H-phenoxazin-3-one)nitratosilver(I). For complex [Ag(Phx-1)$_2$NO$_3$] preparation, an ethanolic solution (5 cm^3) of $AgNO_3$ (0.2 mmol, 0.0339 g) was added to Phx-1 (0.2 mmol, 0.0454 g) dissolved in 10 cm^3 of ethanol (333 K). The reaction mixture was stirred and heated at 333 K for a few minutes in a temperature-controlled bath. From the resulting orange solution, stored in a beaker covered with parafilm, the orange crystals precipitated the next day. After a few days, crystals were washed abundantly with ethanol and dried at room temperature. Yield: 0.13 g, 0.20 mmol (36% based on $AgNO_3$]). Anal. Calcd. for $C_{28}H_{28}Ag_1N_5O_7$ (%): C, 51.39; H, 4.31; N, 10.70. Found: C, 52.84; H, 4.26; N, 10.76.

^{1}H NMR (DMSO-d$_6$, 600 MHz): 7.24 (d, ^3J = 7.9 Hz, 1 H, H-9), 6.84 (dd, ^3J = 7.9 Hz, ^4J = 1.1 Hz, 1 H, H-8), 6.80 (s, 2 H, NH$_2$), 6.76 (d, ^4J = 1.1 Hz, 1 H, H-6), 6.14 (s, 1 H, H-1), 3.27 (d, ^2J = 15.9 Hz, 1 H, H-4a), 3.05 (d, ^2J = 15.9 Hz, 1 H, H-4b), 2.27 (s, 3 H, MeC-7), 1.14 (s, 3 H, MeC-4α). ^{13}C NMR (DMSO-d$_6$, 151 MHz): 191.20 (C-3), 162.46 (C-10α), 147.59 (C-2), 143.89 (C-5α), 137.03 (C-7), 131.91 (C-9α), 125.55 (C-9), 123.08 (C-8), 116.66 (C-6), 104.87 (C-1), 71.44 (C-4α), 48.99 (C-4), 22.08 (MeC-4α), 20.79 (MeC-7).

2.3. *X-ray analysis*

Crystallographic measurement was performed on a Xcalibur R automated four-circle diffractometer with graphite monochromated Mo *Kα* radiation at 100(2) K using an Oxford Cryosystems cooler. Selected crystallographic data are provided in table 1. Data collection, cell refinement, and data reduction and analysis were carried out with CRYSALISCCD and CRYSALISRED, respectively [14]. Analytical absorption correction was applied with CRYSALISRED [14]. The structure was solved by direct methods using SHELXS-97 [15] and refined by full-matrix least squares with SHELXL-97 [15], with anisotropic thermal parameters for all non-H atoms (unless otherwise stated below). N-bound H atoms were found in difference Fourier maps, but in the final refinement cycles they were treated with DFIX and AFIX 3 instructions [15] and refined with U_{iso}(H) = 1.2U_{eq}(N). C-bound H atoms were placed in their calculated positions and refined using a riding model, with C–H = 0.95–0.99 Å and U_{iso}(H) = 1.5U_{eq}(CH_3) or 1.2U_{eq}(CH_2, CH). During the refinement, the Ag ion and one of two ligand molecules were disordered and each one was refined over two sites with 0.970(2)/0.030(2) and 0.948(3)/0.052(3) occupancies, respectively. C and O atoms with minor occupancies were refined isotropically and in the final refinement cycles constrained to have equal displacement parameters. ORTEP [16] was used for the creation of figures.

2.4. *Spectroscopic measurements*

The FT-Raman spectra were measured on a Bruker MultiRAM spectrometer equipped with a Nd:YAG laser (1064 nm) and a liquid nitrogen cooled germanium detector. The spectra were recorded (128 scans) at a resolution of 2 cm^{-1} and 250 mW laser power for Phx-1 and 50 mW for complex in the range 3500-50 cm^{-1}. The middle- and far-infrared spectra were measured on a Bruker VERTEX 70V vacuum spectrometer equipped with a diamond ATR accessory and air-cooled DTGS detector. The instrument was kept under vacuum during the measurements, and the spectra were recorded (128 scans) at a resolution of 2 cm^{-1}.

The ^{1}H and ^{13}C NMR spectra were recorded in DMSO-d_6 or CH_3OH-d_4 on a Bruker Avance 600 spectrometer (600 for ^{1}H and 151 for ^{13}C) at 295 K. Chemical shifts (δ) are given in parts per million (ppm) downfield relative to TMS, and coupling constants (*J*) are in Hz.

2.5. *Theoretical studies*

The DFT calculations were performed for the Phx-1 ligand and its [Ag(Phx-1)$_2$NO$_3$] complex using the Gaussian09 program [17]. The respective crystallographic data was used as the starting geometry in the optimization procedure. Full geometry optimizations were performed by means of the three-parameter hybrid B3LYP-D3 [18, 19] method (B3LYP functional corrected with the original D3 damping function [20]) combined with the D95V(d, p) [21] basis set for all ligand atoms. For the Ag atom, the LanL2DZ effective core potential with the concomitant valence basis set was applied [22].

The optimized structure corresponds very well to that measured, as results from table 2 show where selected structural parameters from the X-ray analysis are compared with corresponding calculated values. The RMS difference between measured and calculated skeletal bond lengths is about 0.04 Å whereas for the plane angles it equals 1.7°. The noticeable difference is in the mutual orientation of organic ligands. In the crystalline state, both ligands are almost flat and are positioned close to the same plane. In the optimized structure, the aromatic rings are slightly twisted in relation to the respective chelate rings, which in turn are more twisted in relation to each other.

For the systems investigated, full geometry optimizations were followed by the calculations of theoretical spectra based on vibrational frequencies and infrared intensities or Raman activities. Figures S1 and S2 show the comparison of observed spectra with theoretical ones, calculated for half-band-width equal 5 cm^{-1}. The vibrational assignments of the experimental ligand spectra were accomplished by the examination of the calculated potential energy distribution, PED terms (ligand) and visualization of normal modes (ligand and complex). For better correlation between observed and calculated wavenumbers, the latter were scaled by a 0.97 factor, except for the NO_3 group vibrations, for which the correlation was satisfactory.

2.6. *In vitro antibacterial assay*

The antimicrobial activities of tested compounds were determined using a modified two-fold microdilution procedure [23] and presented in *Minimum Inhibitory Concentration* values (MIC, mg·dm^{-3}). The MIC was defined as the lowest concentration of tested compound that inhibited the visible growth of microorganism after 24 h of incubation in defined cultivation conditions.

2.6.1. Microorganisms and inocula preparation. The biological activity of each compound was tested against Gram-positive and Gram-negative bacterial strains. The Gram-positive microorganisms such as *Staphylococcus aureus* (PCM 2054), *Bacillus licheniformis* (PCM 1847), *Rhodococcus erythropolis* (PCM 2149) and Gram-negative *Escherichia coli* (PCM 2057), *Pseudomonas fluorescens* (PCM 2123), *Alcaligenes faecalis* (PCM 2223) originated from *Polish Collection of Microorganisms*. The strains were cultivated in liquid Mueller-Hinton medium (MH) with the composition of $g \cdot dm^{-3}$: beef extract, 2; casein hydrolysate, 17.5; starch, 1.5; pH 7.2. All chemicals were of high purity grade used for microbiological procedures (Sigma-Aldrich). The bacterial liquid cultures (inocula) were carried out in 250 cm^3 glass flasks closed with cotton plugs. The flasks contained 100 cm^3 of the MH medium with appropriate microorganism and were agitated on rotary-shaker with 120 rpm at 32 °C. Growth of the culture was monitored by spectrophotometric measurements of an optical density at 600 nm until it reached a logarithm phase growth which corresponded to OD_{600} between 0.4-0.6. Subsequently, a microbial cell suspension was diluted to obtain the final optical density at 0.02 and used as an inoculum to antimicrobial activity evaluation.

2.6.2. MIC evaluation. The compounds in the crystalline form, $[Ag(Phx\text{-}1)_2NO_3]$ and $AgNO_3$, or as powders, 2-amino-4,4α-dihydro-4α,7-dimetylo-3H-phenoxazine-3-one (Phx-1) and 2-amonophenoxazine-3-one (Questiomycin A), were dissolved in DMSO. Such prepared stock solutions were further dissolved in the MH medium to obtain the 5.0% (*v/v*) concentration of the DMSO. The serial microdilutions of tested compounds were performed in 96 microwell plates with the same cultivation medium, in the range of concentrations varied from 0.183 to 375 $mg \cdot dm^{-3}$. Each well containing 0.1 cm^{-3} of diluted compound was then inoculated with 0.005 cm^{-3} of previously prepared diluted bacterial cell suspension. Next, the 96-microwells plates were incubated for 24 h in the dark at 32 °C, after which, the results were noted. The plates were further incubated at the same condition for the next 24 h to confirm the former results. Similar experiments were conducted for DMSO (positive control) at an initial concentration of 5.0% (*v/v*) to exclude a toxic effect on microbial growth of the applied solvent. Nifuroxazide and chloramphenicol were used as reference standards (negative controls) for representative Gram-negative and Gram positive, *E. coli* and *S. aureus* strains, respectively. All experiments were performed in duplicate. The assays performed in duplicate and resulting in the

same MIC values were assumed as correct. Additional two assays were carried out in a case of inconsistent results. In such cases, the mean values of all (four) tests were taken as final results and standard deviations were calculated as the error analysis. Such procedures were carried out for [Ag(Phx-1)$_2$NO$_3$] tested towards *A. faecalis*, Phx-1 against *B. licheniformis*, AgNO$_3$ towards *E. coli* and questiomycin A against all Gram positive bacteria. For these experiments, table 3 lists the mean MIC values and standard deviations. All results of MIC measurements are included in table S1 (Supplementary Material).

3. Results and discussion

3.1. *Molecular structure and crystal packing*

The crystal structure of the investigated complex is slightly complicated by two effects, disorder of the silver ions and the presence of two complex isomers, due to the chirality of the ligand. Both effects are relatively small, which may be illustrated by respective occupancies. The minor occupancy of Ag(I) site is 3.0(2)% whereas the second complex isomer contributes 5.2(3)%. Both effects will be omitted in the figures and tables for better clarity. The refinement did not reveal any disorder of the nitrate ion position. The fact seems surprising, yet a ~5% minor occupancy would require refinement of less than half of an electron. The disordered position of the nitrate ion might lie to close to the major occupancy to be detected and refined.

The structure of discrete [Ag(Phx-1)$_2$(NO$_3$)] entity is shown in figure 2. The central ion is coordinated by two organic ligands acting in monodentate mode and one oxygen atom of the nitrate counterion. The Ag(I) ion environment is close to planar with the metal ion being the most separated from the best N10a-Ag-O1-N10b plane by 0.153 Å or by 0.213 Å from N10a-O1-N10b plane. However, the mutual location of coordination centers is not symmetric, as seen from the angles: N10a-Ag-N10b = 156.18(8), N10a-Ag-O1 = 83.20(8) and N10b-Ag-O1 = 116.64(8). The sum of these angles is 356.02, which again confirms the quasi-planarity of the metal coordination vicinity.

The second Ag1 site is 0.58(2) Å from the original Ag(1) and located closer to the N10b atom, which makes the Ag1-N bond lengths more different (Ag1-N10a 2.277(13) Å, Ag1-N10b 2.060(11) Å).

The main part of the ligand skeleton is formed by three 6-membered rings, one of aromatic character (R3 in figure 2). The two remaining rings lie very close to the plane of the

aromatic one. The largest displacement from the aromatic ring best plane is the C41a atom (0.498 Å). The next largest is the C3a atom with 0.214 Å displacement. Similar parameters for second ligand are 0.728 Å (C41b) and 0.936 Å (C3b). Other small structural differences between the ligand molecules can be deduced from table 2, where corresponding ligand parameters are listed. In ligand skeletal bond lengths, the largest difference is 0.013 Å, found for the C41a–O5a bond and its counterpart. The O5a and O5b atoms also form one of the most different angles C41x–O5x–C51x (x = a or b) for which the difference is 2.3°. The 29.4° difference between C9x–C91x–N10x–Ag angles points out that two organic ligands present in the complex are twisted relative to each other. This is also demonstrated by the dihedral angle of 46.2°, measured between the best planes composed for each ligand of all ring skeletal atoms, except C41a or C41b.

Comparison with the structure of pure Phx-1 ligand [13] shows that formation of Ag-N10a/b bonds caused very small changes in the vicinities of coordinating nitrogen atoms. The C11a/b-N10a/b and N10a/b-C91a/b bonds enlarged less than 0.5%, whereas the C11a/b-N10a/b-C91a/b angles changed less than 0.4%.

The orientation of the nitrate group, represented by the N1-O2-O3 plane, is fixed by five hydrogen bonds with O2 and O3 atoms as acceptors. Among these is one intramolecular C9b-H9b···O2 hydrogen bond of C9b···O2 distance = 3.414(4) Å. Probably by mere coincidence, the nitrate plane lies very close to the plane of aromatic ring C51b–C91b (the largest separation of 0.132 Å was found for the O2 atom).

The crystal packing is stabilized by nine intermolecular hydrogen bonds of N–H and C–H donor types. The strongest connection between complex molecules is via N1a-H3a···O2^{i} N1b-H3b···O1^{i} and N1-bH2b···O2^{ii} hydrogen bonds (D···A 2.993(3), 2.928(3) and 3.200(3) Å, respectively). Interactions are visualized in figure 3 (the caption of this figure contains the corresponding symmetry codes). These bonds organize molecules related by the 2-fold screw axis symmetry operation into chains extending along the *b* axis, as shown in figure 3. Additional stabilization is provided by C–H···O interactions (not shown in figure 3). Weaker C4b-H4b2···O1a^{iii} bonds (3.470(3) Å, symmetry code: (iii) x+1/2, 1/2-y, z-1/2) join the chains into planes parallel to (1 0 1) plane. The planes are connected in a three-dimensional network by C13a-H13a···O1^{iv} bonds (3.451(3) Å; symmetry code (iv) x-1/2, 3/2-y, z-1/2).

3.2. *Vibrational spectroscopy*

In the spectroscopic part of the present work, the vibrational spectra of pure Phx-1 ligand and its Ag(I) complex were compared for tracing the changes caused by metal coordination. Special attention was focused on skeletal stretching vibrations absorbing mainly in the 1800 – 600 cm^{-1} region, shown in figure 4. The band assignment was made with the help of DFT calculated frequencies, which show about 12 cm^{-1} RMS observed – calculated differences in the mentioned region.

The monodentate coordination mode of the Phx-1 ligand suggests that the vibrations of the C11a=N10a-C91a subgroup (atom numbering as in figure 2) should be the most affected by metal bonding. However, as results from the calculations indicate, it is difficult to find IR bands characteristic for the stretching ν(C11a=N10a) or ν(C91a-N10a) vibrations. For a conjugated system such as the Phx-1 skeleton, most stretching skeletal vibrations are strongly coupled and involve simultaneous motion of many atoms. This is confirmed by PED analysis where the largest contribution of particular internal stretching modes is typically less than 30% (except ν(C=O) with 70% contribution). The largest contributions of the ν(C11a=N10a) internal mode have been found in normal vibrations of Phx-1 at 1565 and 1554 cm^{-1} (for respective PED values see table 4). Similar character show two normal vibrations calculated for $[Ag(Phx\text{-}1)_2(NO_3)]$ complex at about 30 cm^{-1} lower wavenumbers (1536 and 1523 cm^{-1}). In the 1600 – 1500 cm^{-1} region of the observed IR spectra the Phx-1 bands at 1587 and 1533 cm^{-1} show the largest downshift upon coordination (1574 and 1528 cm^{-1} in the complex spectrum) and these bands have been assigned to vibrations with a substantial ν(C=N) contribution.

The stretching vibration of the neighboring C91a-N10a bond is more dispersed over several normal modes, with maximum contribution of 22% in 1217 cm^{-1} vibration. For two ligand molecules present in the complex, the similar ν(C-N) mode was calculated at 1222 and 1218 cm^{-1}. For these vibrations, the bands observed at 1229 and 1231 cm^{-1} have been proposed. Other normal vibrations with PED contributions of oxazine ring stretching modes exceeding 5% can be found in table 4.

The most visible spectral change caused by metal coordination is the splitting of characteristic ν(C=O) vibration. In Phx-1, this vibration generates the strong IR band at 1692 cm^{-1}, whereas in the complex spectrum, two bands at 1711 and 1696 cm^{-1} are observed. Similar splitting was predicted by calculations, pointing out that two ligand subunits present in

the complex are not structurally and spectrally equal. The first difference is confirmed by the X-ray analysis showing that the C=O bond lengths are slightly different (table 2) and only one C3a=O1a group is involved in hydrogen bonding, as an acceptor. The second difference is monitored by calculated PED terms. In both ν(C=O) normal vibrations the C=O stretching mode contributes in 70%, but remaining contributions are different, for example: 5% of bending δ(C1b-C2b-C3b) for higher wavenumber vibration and 4% of ν(C3a-C4a) for lower one.

The new spectral features caused by metal coordination are the bands resulting from so called "metal-ligand" vibrations. For the presented complex, these vibrations are expected at low wavenumbers because of the Ag atomic mass and stiffened motion of coordinating nitrogen atoms mounted into ring systems. Animation of calculated normal vibrations demonstrates that the simultaneous stretching of both Ag-N bonds is connected with motions of whole Phx-1 ligands. The largest amplitudes has been found for 74 and 167 cm^{-1} normal vibrations (symmetric ν_s(Ag-N)) and for 116 and 174 cm^{-1} modes (asymmetric ν_a(Ag-N)). Such vibrations may contribute in respective bands at 76, 118 and 177 cm^{-1} found in the FIR spectrum of the [Ag(Phx-1)$_2$(NO_3)] complex. Changes of Ag-N bond length have also been observed for oxazine ring deformations with large nitrogen atom displacements, calculated at 450 and 455 cm^{-1} and attributed to 452 cm^{-1} band. The Ag-O distance changes significantly when whole NO_3 group is displaced, as in normal vibration at 155 cm^{-1}, or during NO_3 in-plane bending vibrations, calculated at 712 and 695 cm^{-1}. First vibration was assigned to 155 cm^{-1} IR shoulder; two remaining modes will be discussed latter.

The NO_3 group vibrations have been localized by comparison of the literature data with respective regions of complex and additionally the ligand spectra. In the former, additional IR bands were found at 1426, 1383, 1042, 823, 736 and 715 cm^{-1} corresponding to ν_3, ν_3, ν_1, ν_2 and ν_4, ν_4, vibrations of simple nitrate salts [24]. The splitting of the ν_3 and ν_4 modes (doubly degenerated in free NO_3^- ion) and IR activity of ν_1 mode confirm the symmetry lowering of nitrate ion upon metal coordination.

The foregoing discussion, and those bands listed in table 4, do not cover all vibrations of Phx-1 and its silver complex. As predicted for Phx-1 by DFT calculations, about 40% of total 90 normal vibrations have weak IR intensity, being more than 50 times lower than the intensity of strong ν(C=O) band at 1694 cm^{-1}, taken for example as a reference. The wavenumbers of many of these transitions are not available because of the overlap by stronger ones. In the case of the

$[Ag(Phx\text{-}1)_2(NO_3)]$ complex, which molecule has 201 normal vibrations, the number of observed bands is not significantly increased because two coordinating ligand molecules have very close wavenumbers of corresponding vibrations.

3.3. *In vitro antibacterial assay*

The comparative biological studies of the $[Ag(Phx\text{-}1)_2NO_3]$ complex as well as remaining reference compounds such as $AgNO_3$ and Phx-1, and Questiomycin A, both prepared at enzymatic procedures and other antibiotics were performed against Gram-positive and Gram-negative bacteria, applying commonly known microdilution procedure. The antibacterial activities, presented in MIC values, are included in table 3.

The MIC values of the various organic ligands, the silver(I) salt and its coordination compound can vary significantly between applied procedures [25, 26], bacteria species or even between the strains, as found in the literature [27-29]. Nevertheless, an effort to perform a comparable qualitative analysis of the obtained data has been made.

Results from table 3 show the Phx-1 ligand exhibited lack of activity against Gram-negative representatives and only very weak action towards some Gram-positive bacteria. Comparing these results to the Phx-1 analog, Questiomycin A, the latter presented weak antibacterial action towards Gram-positive strains, especially for *S. aureus* and *R. erythropolis*. Similar results were obtained by Shimizu and co-workers [30] who investigated the antibacterial activity of these two phenoxazine derivatives on mycobacteria and other bacteria strains, applying similar microdilution method. In their research both compounds did not present biological action against *E. coli* and *S. aureus*, in tested range of concentrations with the maximum saturation at 45 $mg \cdot dm^{-3}$. The lack of antimicrobial activity for both organic molecules could be attributed to a phenoxazine system, which probably easily undergoes inactivation during the metabolic pathways. The hydroxylation of heterocyclic aromatic rings is a typical and essential step in carbon cycle [31] and defense mechanism of the microorganisms when exposed on unfriendly environment [32, 33].

Further comparison of the results obtained for tested compounds showed that the complexation of silver nitrate lead to appreciably improved activities of the organic ligand Phx-1. For selected Gram-positive and Gram-negative representatives the antibacterial activity of the complex was significantly enhanced in comparison to pure ligand, respectively. Thus, the

$[Ag(Phx\text{-}1)_2NO_3]$ compound presents a wide spectrum of the biological activity against both Gram-positive and Gram-negative bacteria in the investigated range of concentrations (0.183-375 $mg \cdot dm^{-3}$). The minimum inhibitory concentrations corresponded to *E. coli*, *P. fluorescens* (23 $mg \cdot dm^{-3}$) and *S. aureus*, *B. licheniformis* strains (47 $mg \cdot dm^{-3}$) are of the same order of magnitude, indicating comparable antibacterial activity. However, in these two groups of microorganisms, there are strains which do not follow the tendency being more resistant (*A. faecalis)* or more sensitive (*R. erythropolis)* to tested coordination compound. Different results were obtained [28], where the authors investigated the beneficial effect of Questiomycin A complexation with silver(I) nitrate. The resulted coordination compound [Ag(2-aminophenoxazine-3-one)(NO_3)] presents enhanced biological activity only against *S. aureus* in comparison to pure ligand and inorganic salt.

Figure 5 clearly shows that the biological activity of $[Ag(Phx\text{-}1)_2NO_3]$ is predominantly an effect of the metal cation action. For all tested microorganisms, the $AgNO_3$ solution exhibited very strong toxic effect, which remains in agreement with the literature data [34-36]. Silver is an antimicrobial agent of medical application due to its non-toxicity for human cells. An excellent example of its usage is silver(I)-sulfadiazine, a polymeric drug commonly used on a wound surface of scalded skin to accelerate healing and simultaneously prevent bacterial infections [37]. The inhibitory action of silver and its compound on microorganisms is poorly understood. Nevertheless, recent research provides some possible explanations of antibiological mechanisms. In the mechanisms mentioned, the following are frequently listed: damage of cell membrane and interaction with protein having thiol groups or with active side of enzymes. Jung and co-workers [34] performed a detailed study on antibacterial effect of silver(I) solution on *E. coli* and *S. aureus* by analyzing the growth and structure of bacterial cell. They concluded that silver cation exhibited better activity towards gram-negative rather than gram-positive bacteria due to the differences in cell membrane morphology. The exposition of cell on silver solution caused cell wall damage and separation of cellular components from microbial membrane. The additional studies were conducted on possible interactions of Ag(I) ion with sulfhydryl (thiol) or imidazole groups present in various organic compounds [36, 38] as well as in amino acid polymeric chains in enzymes and other proteins [29, 37, 39]. Above examples showed that antibacterial properties of silver cation can affect various processes inside the microbial cell.

In summary, based on the obtained MICs, the antibacterial activity should be classified

rather as moderate in comparison to values of tested antibiotics such as chloramphenicol (2.9 mg dm^{-3}) and nifuroxazide (0.73 mg dm^{-3}). Nevertheless, among tested microorganisms were strains (*R. erythropolis*, *B. licheniformis*) of better antibacterial activity than for $AgNO_3$ and are comparable to chloramphenicol. Thus, the group of Gram-positive bacteria should be further tested as potential group sensitive for $[Ag(Phx\text{-}1)_2NO_3]$ complex.

4. Conclusion

Silver(I) complex with phenoxazine derivative (Phx-1) has been synthesized and characterized by X-ray, IR and Raman and biological methods. The ligand acts in monodentate mode, binding the silver(I) ion via nitrogen atom of phenoxazine ring. Due to ligand chirality, the obtained $[Ag(Phx\text{-}1)_2NO_3]$ crystals are composed mainly of complex molecules with R and one S enantiomers; only about 5% of molecules are built of the same enantiomers.

Binding the Ag(I) ion causes very small changes (less than 0.5%) in lengths of bonds around coordinating nitrogen atom. Nevertheless, the respective vibrations changed significantly shifting to lower wavenumbers, which suggests that this is mostly due to the "mass effect" of heavy metal attachment to the nitrogen atom. The $[Ag(Phx\text{-}1)_2NO_3]$ complex shows moderate antibacterial activity in comparison with some commercial antibiotics, but exhibits better antibacterial activity than for Phx-1 or $AgNO_3$ for selected Gram-positive bacteria. This observation confirms the hypothesis that metal complexation may enhance the biological activity of the used ligand or metal salt.

Supplementary material

CCDC 1525422 contains the supplementary crystallographic data for this paper. The data can be obtained free of charge from the Cambridge Crystallographic Data Centre via www.ccdc.cam.ac.uk/structures.

Acknowledgements

This work was financed in part by a statutory activity subsidy from the Polish Ministry of Science and Higher Education for the Faculty of Chemistry of Wroclaw University of Technology. A generous computer time from the Wroclaw Supercomputer and Networking Center as well as the Poznan Supercomputer and Networking Center is acknowledged.

References

[1] U. Hollstein. *Chem. Rev.*, **74**, 625 (1974).

[2] A. Tomoda, K. Miyazawa, T. Tabuchi. *Int. J. Mol. Sci.*, **14**, 17573 (2013).

[3] K. Kimura, Y. Usui, T. Hattori, N. Yamakawa, H. Goto, M. Usui, S. Okada, K. Shirato, A. Tomoda. *Oncol. Rep.*, **19**, 3 (2008).

[4] S. Kato, K. Shirato, K. Imaizumi, H. Toyota, J. Mizuguchi, M. Odawara, X.-F. Che, S. Akiyama, A. Abe, A. Tomoda. *Oncol. Rep.*, **15**, 843 (2006).

[5] N. Miyano-Kurosaki, K. Ikegami, K. Kurosaki, T. Endo, H. Aoyagi, M. Hanami, J. Yasumoto, A. Tomoda. *J. Pharmacol. Sci.*, **110**, 87 (2009).

[6] K. Hayashi, T. Hayashi, K. Miyazawa, A. Tomoda. *J. Pharmacol. Sci.*, **114**, 85 (2010).

[7] S. Shimizu, M. Suzuki, A. Tomoda, S. Arai, H. Taguchi, T. Hanawa, S. Kamiya. *Tohoku J. Exp. Med.*, **203**, 47 (2004).

[8] Y. Zhao, X. Yang, J. Tian. *Electrochim. Acta*, **54**, 7114 (2009).

[9] Y. Zhao, X. Yang, J. Tian, F. Wang, L. Zhan. *Mater. Sci. Eng., B*, **171**, 109 (2010).

[10] K. Pandurangan, S. Gallagher, G.G. Morgan, H. Müller-Bunz. F. Paradisi. *Metallomics*, **2**, 530 (2010).

[11] M. Giurg, K. Piekielska, M. Gębala, B. Ditkowski, M. Wolański, W. Peczyńska–Czoch, J. Młochowski. *Synth. Commun.*, **37**, 1779 (2007).

[12] J.M. Granda, K. Piekielska, M. Wąsińska, N. Kawecka, M. Giurg. *Synthesis*, **47**, 3321 (2015).

[13] S.M. Jansze, V. Saggiomo, A.T.M. Marcelis, M. Lutz, A.H. Velders. *Tetrahedron Lett.*, **56**, 1060 (2015).

[14] Oxford Diffraction, CrysAlis CCD and CrysAlis RED in Xcalibur PX and Kuma KM-4-CCD Software, Oxford Diffraction Ltd., Yarnton, Oxfordshire, England (2009).

[15] G.M. Sheldrick. *Acta Crystallogr.*, **A64**, 112 (2008).

[16] L.J. Farrugia. *J. Appl. Cryst.*, **30**, 565 (1997).

[17] M.J. Frisch, G.W. Trucks, H.B. Schlegel, G.E. Scuseria, M.A. Robb, J.R. Cheeseman, G. Scalmani, V. Barone, B. Mennucci, G.A. Petersson, H. Nakatsuji, M. Caricato, X. Li, H.P. Hratchian, A.F. Izmaylov, J. Bloino, G. Zheng, J.L. Sonnenberg, M. Hada, M. Ehara, K. Toyota, R. Fukuda, J. Hasegawa, M. Ishida, T. Nakajima, Y. Honda, O. Kitao,

H. Nakai, T. Vreven, J.A. Montgomery Jr., J.E. Peralta, F. Ogliaro, M. Bearpark, J.J. Heyd, E. Brothers, K.N. Kudin, V.N. Staroverov, R. Kobayashi, J. Normand, K. Raghavachari, A. Rendell, J.C. Burant, S.S. Iyengar, J. Tomasi, M. Cossi, N. Rega, J.M. Millam, M. Klene, J.E. Knox, J.B. Cross, V. Bakken, C. Adamo, J. Jaramillo, R. Gomperts, R.E. Stratmann, O. Yazyev, A.J. Austin, R. Cammi, C. Pomelli, J.W. Ochterski, R.L. Martin, K. Morokuma, V.G. Zakrzewski, G.A. Voth, P. Salvador, J.J. Dannenberg, S. Dapprich, A.D. Daniels, O. Farkas, J.B. Foresman, J.V. Ortiz, J. Cioslowski, D.J. Fox, Gaussian, Inc., Wallingford, CT (2009).

[18] A.D. Becke. *J. Chem. Phys.*, **98**, 5648 (1993).

[19] C. Lee, W. Yang, R.G. Parr. *Phys. Rev. B*, **37**, 785 (1988).

[20] S. Grimme, J. Antony, S. Ehrlich, H. Krieg. *J. Chem. Phys.*, **132**, 154104 (2010).

[21] T.H. Dunning Jr., P.J. Hay. In *Modern Theoretical Chemistry*, H.F. Schaefer (Ed.), Vol. 3, pp. 1-28. Plenum Press, New York (1976).

[22] P.J. Hay, W.R. Wadt. *J. Chem. Phys.*, **82**, 299 (1985).

[23] EUCAST discussion document. *Clin. Microbiol. Infect.*, **9**, 1 (2003).

[24] K. Nakamoto, *Infrared and Raman Spectra of Inorganic and Coordination Compounds*, Part A, p. 183, John Wiley & Sons, Hoboken (2009).

[25] I. Chopra. *J. Antimicrob. Chemother.*, **59**, 587 (2007).

[26] S. Zhang, L. Liu, V. Pareek, T. Becker, J. Liang, S. Liu. *J. Microbiol. Methods*, **105**, 42 (2014).

[27] M. Cavicchioli, A.C. Massabni, T.A. Heinrich, C.M. Costa-neto, E.P. Abrão, B.A.L. Fonseca, E.E. Castellano, P.P. Corbi, W.R. Lustri, C.Q.F. Leite. *J. Inorg. Biochem.*, **104**, 533 (2010).

[28] K. Pandurangan, S. Gallagher, G.G. Morgan, H. Mu. *Metallomics*, **5901**, 4 (2010).

[29] U. Kalinowska-Lis, A. Felczak, L. Che, K. Lisowska, J. Ochocki. *J. Organomet. Chem.*, **749**, 394 (2014).

[30] S. Shimizu, M. Suzuki, A. Tomoda, S. Arai, H. Taguchi, T. Hanawa, S. Kamiya. *Tohoku J. Exp. Med.*, **203**, 47 (2004).

[31] W.C. Evans. *J. Gen. Microbiol.*, **32**, 177 (1963).

[32] R. Ullrich, M. Hofrichter. *Cell. Mol. Life Sci.*, **64**, 271 (2007).

[33] P. Di Gennaro, A. Bargna, G. Sello. *Appl. Microbiol. Biotechnol.*, **90**, 1817 (2011).

[34] W.K. Jung, H.C. Koo, K.W. Kim, S. Shin, S.H. Kim, Y.H. Park. *Appl. Environ. Microbiol.*, **74**, 2171 (2008).

[35] C.P. Randall, L.B. Oyama, J.M. Bostock, I. Chopra, A.J.O. Neill. *J. Antimicrob. Chemother.*, **68**, 131 (2013).

[36] K. Nomiya, Y. Kondoh, K. Onoue, N.C. Kasuga, H. Nagano, M. Oda, T. Sudoh, S. Sakuma. *J. Inorg. Biochem.*, **58**, 255 (1995).

[37] C.G. De Gracia. *Burns*, **27**, 67 (2001).

[38] K. Nomiya, K. Tsuda, T. Sudoh, M. Oda. *J. Inorg. Biochem.*, **68**, 39 (1997).

[39] R.B. Wakshlak, R. Pedahzur, D. Avnir. *Sci. Rep.*, **5**, 1 (2015).

Table 1. Crystal data, data collection and refinement details for $[Ag(Phx\text{-}1)_2NO_3]$.

Compound	$[Ag(Phx\text{-}1)_2NO_3]$
Empirical formula	$C_{28}H_{28}AgN_5O_7$
Formula weight	654.42
Crystal system	Monoclinic
Space group	$P2_1/n$
a (Å)	15.258(5)
b (Å)	10.895(3)
c (Å)	17.338(5)
β (°)	111.73(5)
Volume (Å^3)	2677.4(16)
Z (molecule/cell)	4
D_{calc} (Mg m^{-3})	1.624
F(000)	1336
Crystal size (mm)	0.15 × 0.12 × 0.06
Wavelength (Å)	0.71073
Temperature (K)	100(2)
θ range (°)	2.874–30.796
Absorption coefficient (mm^{-1})	0.810
Index ranges (limiting indices)	$-21 \le h \le 13$ $-15 \le k \le 13$ $-24 \le l \le 24$
Reflection collected / unique (R_{int})	18407 / 7577 [R_{int} = 0.040]
Goodness-of-fit	1.039
Final R indices [$I>2\sigma(I)$]]	R_1=0.0433, wR_2=0.0716
R indices (all data)	R_1=0.0679, wR_2=0.0790
Largest diff. peak and hole (e Å^{-3})	0.59 and -0.42

Table 2. Selected bond lengths [Å] and angles [°] of $[Ag(Phx\text{-}1)_2NO_3]$ with e.s.d.s. in parentheses. Aromatic ring parameters are omitted as being close to typical.

Parameter	X-ray	DFT	Parameter	X-ray	DFT
Ag–N10a	2.193(2)	2.363	Ag–N10b	2.161(2)	2.304
Ag–O1	2.573(2)	2.501	N1–O1	1.257(2)	1.275
N1–O2	1.256(2)	1.278	N1–O3	1.239(2)	1.254
Ligand “a”			Ligand “b”		
C1a–C2a	1.358(3)	1.382	C1b–C2b	1.368(3)	1.375
C1a–C11a	1.416(3)	1.418	C1b–C11b	1.417(3)	1.433
C2a–N1a	1.344(3)	1.349	C2b–N1b	1.336(3)	1.363
C2a–C3a	1.491(3)	1.504	C2b–C3b	1.498(3)	1.501
C3a–O1a	1.213(3)	1.224	C3b–O1b	1.208(3)	1.225
C3a–C4a	1.501(3)	1.517	C3b–C4b	1.498(3)	1.514
C4a–C41a	1.518(3)	1.532	C4b–C41b	1.519(4)	1.532
C41a–O5a	1.447(3)	1.449	C41b–O5b	1.434(3)	1.442
C41a–C11a	1.516(3)	1.528	C41b–C11b	1.518(3)	1.528
C41a–C12a	1.521(3)	1.539	C41b–C12b	1.526(4)	1.540
O5a–C51a	1.375(3)	1.368	O5b–C51b	1.377(3)	1.372
C51a–C91a	1.386(3)	1.417	C51b–C91b	1.395(3)	1.411
C7a–C13a	1.498(3)	1.513	C7b–C13b	1.506(4)	1.512
C91a–N10a	1.413(3)	1.402	C91b–N10b	1.407(3)	1.407
N10a–C11a	1.303(3)	1.320	N10b–C11b	1.306(3)	1.311
C1a–C2a–C3a	119.9(2)	119.6	C1b–C2b–C3b	119.3(2)	120.2
C1a–C2a–N1a	125.6(2)	123.6	C1b–C2b–N1b	125.5(2)	124.6
C2a–C3a–C4a	116.3(2)	115.7	C2b–C3b–C4b	115.5(2)	116.7
C2a–C3a–O1a	120.8(2)	120.9	C2b–C3b–O1b	121.0(2)	120.4
C3a–C4a–C41a	112.4(2)	112.7	C3b–C4b–C41b	111.6(2)	114.6
C4a–C41a–O5a	103.8(2)	105.1	C4b–C41b–O5b	105.3(2)	104.4
C4a–C41a–C12a	112.3(2)	111.4	C4b–C41b–C12b	111.5(2)	111.9
C41a–O5a–C51a	114.0(2)	113.9	C41b–O5C–C51b	111.7(2)	114.5
O5a–C51a–C6a	118.5(2)	119.2	O5b–C51b–C6b	119.7(2)	119.1
C6a–C7a–C13a	120.6(2)	120.4	C6b–C7b–C13b	120.8(3)	120.8
C9a–C91a–N10a	120.7(2)	121.6	C9b–C91b–N10b	121.3(2)	121.1
C91a–N10a–C11a	117.8(2)	117.4	C91b–N10b–C11b	117.2(2)	118.1
C91a–N10a–Ag	117.62(15)	123.2	C91b–N10b–Ag	114.94(15)	120.2
N10a–C11a–C1a	121.1(2)	120.9	N10b–C11b–C1b	121.0(2)	120.7
C11a–C1a–C2a	123.5(2)	122.8	C2b–C1b–C11b	122.8(2)	123.3
N1a–C2a–C3a–O1a	14.0(4)	6.0	N1b–C2b–C3b–O1b	-15.3(4)	-3.8
C2a–C3a–C4a–C41a	-40.1(3)	-39.8	C2b–C3b–C4b–C41b	46.3(3)	33.3
C3a–C4a–C41a–C12a	-73.5(3)	-74.0	C12b–C41b–C4b–C3b	72.7(3)	76.8
C51a–C6a–C7a–C13a	-179.6(2)	-178.2	C51b–C6b–C7b–C13b	179.1(4)	178.7

Table 3. The MIC values [mg dm^{-3}] corresponding to presented complex and reference compounds, tested against Gram-negative and Gram-positive bacteria. Standard deviations are given when MIC was calculated as a mean value of four tests.

	Phx-1		Questiomycin A		$[Ag(Phx\text{-}1)_2NO_3]$		$AgNO_3$	
	MIC	SD	MIC	SD	MIC	SD	MIC	SD
E. coli (G-)	>375		82	20	23		5.2	1.3
P. fluorescens (G-)	>375		>375		23		5.9	
A. faecalis (G-)	>375		>375		164	41	23	
S. aureus (G+)	>375		59	20	47		12	
B. licheniformis (G+)	234	81	234	81	47		94	
R. erythropolis (G+)	375		35	12	5.9		12	

MIC of reference samples: nifuroxazide tested against S. aureus – 0.73 mg dm^{-3}; chloramphenicol tested against *E. coli* – 2.9 mg dm^{-3}.

Table 4. Comparison of the selected experimental and the theoretical IR and Raman bands of Phx-1 ligand an its Ag(I) complex.

Phx-1				$[Ag(Phx\text{-}1)_2NO_3]$			
IR	*R*	*DFT*	*PED [%]**	*IR*	*R*	*DFT*	*General assignment**
3399	no	3619	ν(N1-H3)-67 - ν(N1-H2)-25	3452, 3375	no	3594, 3557	$\nu_a(NH_2)$
3286	no	3485	ν(N1-H2)-52 + ν(N1-H3)-33	3288, 3219	no	3469, 3345	$\nu_s(NH_2)$
1694	1693	1704	ν(C=O)-70	1710, 1694	1711, 1696	1722, 1712	ν(C=O)
1623	1619	1612	ν(C1=C2)-24 + ν(C2-N1)-7	1630_{sh}	no	1624	$\nu(C=C)_{R1}$ + ν(C-N)
1617_{sh}	no	1612	ν(C1=C2)-16 + **ν(C11=N10)-9**	1617	1619	1613	$\nu(C=C)_{R1}$ + **ν(C=N)**
1587	1591	1566	**ν(C11=N10)-21** + ν(C9-C91)-13	1574	1577	1536	**ν(C=N)**
1579_{sh}	no	1558	$\delta(NH_2)$-57	no	no	1562	$\delta(NH_2)$
1533	1534	1554	**ν(C11=N10)-31** + ν(C7-C8)-11	1529	1532	1523	**ν(C=N)**
1490	1492	1473	ν(C6-C7)-10 + ν(C9-C91)-9 + **ν(C91-N10)-8**	1489	1491	1475	$\nu(C\text{-}C)_{R3}$ + **ν(C-N)**
1394	1400	1385	ν(C2-C3)-10 + ν(C1-C11)-7	1383	1381	1403	$\nu(C\text{-}C)_{R1}$
1370	1366	1366	$\delta(CH_3)$-57	1370	1365	1367	$\delta(CH_3)$
1354	1353	1342	ν(C1-C11)-14 + ν(C2-N1)-8 + **ν(C11-C41)-7**	1362_{sh}	1365	1353	**$\nu(C\text{-}C)_{R1,R2}$**
1312	1313	1307	ν(C6-C7)-18 + ν(C7-C8)-14 + **ν(C51-C91)-14**	1320	1313	1314	**$\nu(C\text{-}C)_{R3,R2}$**
1288	1289	1273	ν(C4-C41)-9 + **ν(C11-C41)-6**	1284	1287	1279	**$\nu(C\text{-}C)_{R1,R2}$**
1267	1268	1257	**ν(C51-O13)-12** + ν(C7-C13)-9	1269	1266	1263	**ν(C-O)**
1229	1228	1236	**ν(C51-O13)-8** + ν(C2-N1)-7	1231	1232	1247	**ν(C-O)**
1220_{sh}	1222_{sh}	1217	**ν(C91-N10)-22**	1223	1223	1222	**ν(C-N)**
1173	1174	1158	ν(C3-C4)-15 + ν(C12-C41)-7	1173	1177	1162	$\nu(C\text{-}C)_{R1}$
1148	1151	1134	ν(C7-C13)-19 + **ν(C51-O5)-14**	1153	1154	1150	**ν(C-O)**
1125	1126	1116	δ(C8-H)-22 + δ(C9-H)-10	1129	1133	1123	$\delta(C\text{-}H)_{R3}$
1108	1110	1098	**ν(C41-O5)-25**	1107	1109	1099	**ν(C-O)**
1063	1065	1044	$\rho_r(NH_2)$-14 + ν(C12-C41)-11	1053	1055	1059	$\delta_r(NH_2)$
971	972	959	**ν(C41-O5)-11** + ν(C7-C8)-6	972	975	960	**ν(C-O)**
914	915	905	**ν(C41-O5)-15** + ν(C7-C13)-6	920	922	906	**ν(C-O)**
886	no	882	ν(C12-C41)-18	882	884	882	$\nu(C\text{-}CH_3)$
856	856	856	π(C1-H)-92	860	865	857	$\pi(C\text{-}H)_{R1,R3}$
843	no	833	**ν(C91-N10)-6** + **ν(C51-C91)-5**	837	no	843	**ν(C–N)**
812	815	805	π(C8-H)-59 + π(C9-H)-20	808	no	807	$\pi(C\text{-}H)_{R3}$
760	763	773	**δ(C41-O5-C51)-5** + **δ(C11-N10-C91)-5**	763	766	781	**δ(C-O-C) + δ(C=N-C)**
744	745	748	ν(C2-C3)-7 + ν(C7-C13)-7	747	749	748	$\nu(C\text{-}C)_{R1}$
662	665	647	**ν(C11-C41)-7** + ν(C4-C41)-6	672	no	657	**$\nu(C\text{-}C)_{R2}$**
633	no	622	**ν(C11-C41)-5** + δ(C2-C3-O1)-5	645	646	628	**$\nu(C\text{-}C)_{R2}$**
				177, 118	177, 123	169	ν_a(Ag–N)
				143, 76	no	162	ν_s(Ag–N)
				153_{sh}	151	150	ν(Ag–O)
				NO_3			
				1426, no	1425, no	1436, 1330	$\nu_a(NO_3) - \nu_3$
				1042	1043	1035	$\nu_s(NO_3) - \nu_1$
				823	no	789	$\pi(NO_3) - \nu_2$
				736, 715	731, 716	691, 674	$\delta(NO_3) - \nu_4$

* terms related to oxazine ring are boldfaced

Figure captions

Figure 1. Representative aminophenoxazinones with skeleton numbering system of Phx-1.

Figure 2. Molecular structure with thermal ellipsoids at 30% probability and labeling scheme for $[Ag(Phx\text{-}1)_2NO_3]$.

Figure 3. A packing diagram for $[Ag(Phx\text{-}1)_2NO_3]$, showing formation of a molecular chain along the crystallographic *b* axis. Ligands from four neighboring molecules are shown. For the sake of clarity, only N-H···O type hydrogen bonds are shown and hydrogen atoms not involved in H-bonding are omitted. Symmetry codes: (i) 3/2-x, y-1/2, 3/2-z; (ii) x, y-1, z.

Figure 4. Infrared spectra of Phx-1 ligand and its Ag(I) complex in the "fingerprint" region. Bands discussed and listed in table 4 are only labeled; * denotes the NO_3 group vibration.

Figure 5. Comparison of MIC values for all tested Gram-positive and Gram-negative bacteria exposed on $[Ag(Phx\text{-}1)_2NO_3]$ and $AgNO_3$ solutions.

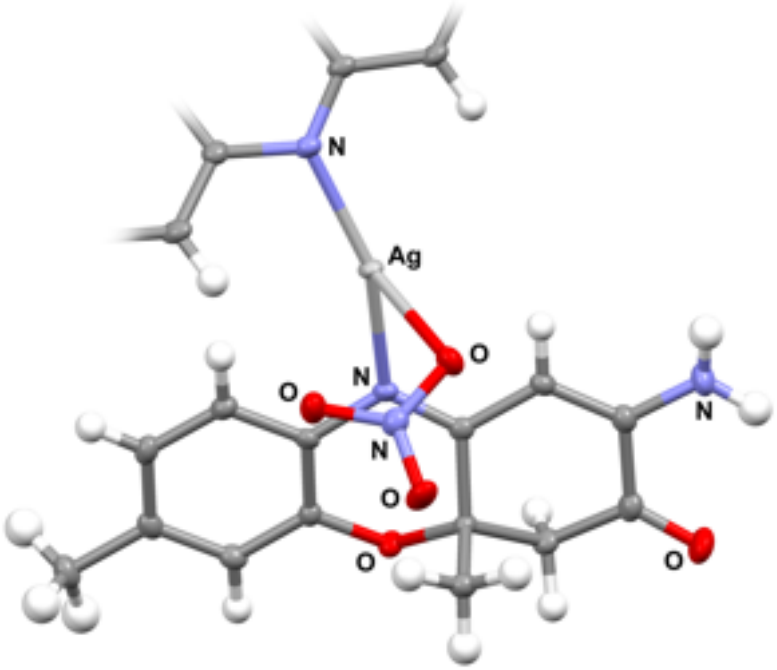

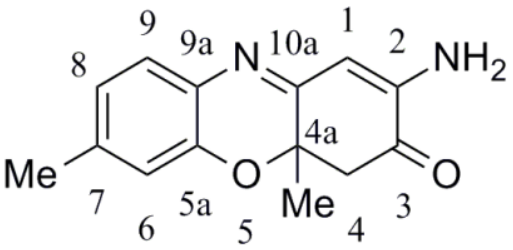

Phx-1

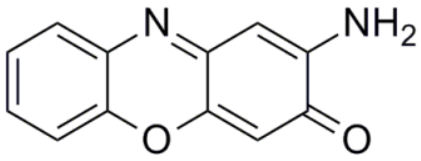

Questiomycin A (Phx-3)

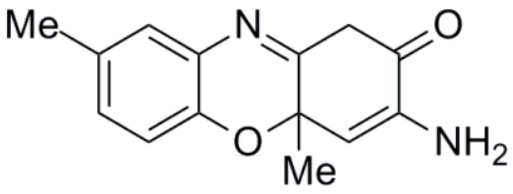

Phx-2

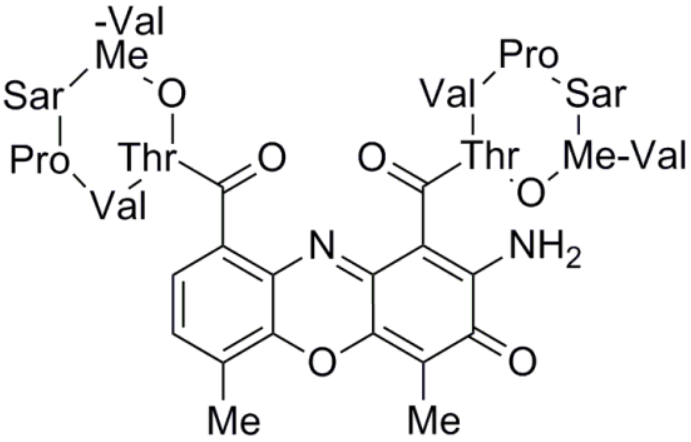

Actinomycin D